Annealing effects on optical properties of low temperature grown ZnO nanorod arrays

Lili Yang, Qingxiang Zhao, Magnus Willander and Ivan Gueorguiev Ivanov

Original Publication:

Lili Yang, Qingxiang Zhao, Magnus Willander and Ivan Gueorguiev Ivanov , Annealing effects on optical properties of low temperature grown ZnO nanorod arrays, 2009, JOURNAL OF APPLIED PHYSICS, (105), 5, 053503.
http://dx.doi.org/10.1063/1.3073993

Annealing effects on optical properties of low temperature grown ZnO nanorod arrays

L. L. Yang,[1,2,a] Q. X. Zhao,[1] M. Willander,[1] J. H. Yang,[2] and I. Ivanov[3]
[1]*Department of Science and Technology (ITN), Linköping University, SE-60174 Norrköping, Sweden*
[2]*Institute of Condensed State Physics, Jilin Normal University, Siping 136000, People's Republic of China*
[3]*Department of Physics, Chemistry and Biology, Linköping University, SE-581 83 Linköping, Sweden*

(Received 25 September 2008; accepted 13 December 2008; published online 4 March 2009)

Vertically well-aligned ZnO nanorods on Si substrates were prepared by a two-step chemical bath deposition method. The structure and optical properties of the grown ZnO nanorods were investigated by Raman and photoluminescence spectroscopy. The results showed that after an annealing treatment at around 500 °C in air atmosphere, the crystal structure and optical properties became much better due to the decrease in surface defects. The resonant Raman measurements excited by 351.1 nm not only revealed that the surface defects play a significant role in the as-grown sample, which was supported by low temperature time-resolved photoluminescence measurements, but also suggested that the strong intensity increase in some Raman scatterings was due to both outgoing resonant Raman scattering effect and deep level defect scattering contribution for ZnO nanorods annealed from 500 to 700 °C. © *2009 American Institute of Physics*.
[DOI: 10.1063/1.3073993]

I. INTRODUCTION

Zinc oxide (ZnO) has generated great interest due to its direct wide band gap of 3.37 eV at room temperature, its large exciton binding energy of 60 meV, and its stable physical and chemical properties. During the past decade, different one-dimensional (1D) ZnO nanostructures such as nanotubes,[1] nanowires,[2] nanorods,[3] nanobelts,[4] nanocables,[5] and nanoribbons,[6] have been successfully fabricated by different methods. Among the methods to prepare 1D ZnO nanorods,[7–13] chemical bath deposition (CBD) appears to have a huge potential for industrial synthesis due to advantages such as easy operation and low temperature fabrication.[14,15] Recently, we successfully controlled the size of well-aligned ZnO nanorod arrays (ZNAs) from 40 to 150 nm with the two-step CBD method,[16] i.e., by first spin coating the substrate with a seed layer of ZnO nanoparticles and then using the CBD growth. However, the applicative use of these ZnO nanostructures requires not only that their crystalline morphology, orientation, and surface architecture be well controlled during the preparation processes but also an improved quality of their optical and electronic properties. Unfortunately, ZNAs grown at a relatively low temperature usually showed poor crystallization and optical properties. However, postannealing may provide an effective way to improve the crystalline quality and the optical properties.[17,18] Therefore, in view of its future applications, it is important to investigate the effects of postannealing on the structure and optical properties of low temperature chemical grown ZNAs.

Resonant Raman scattering (RRS) has been proven to be an important tool for the study of basic physical properties of semiconductors, including nanostructure materials. Multiphonon scattering processes were previously reported for single crystalline bulk ZnO,[19] and recently for ZnO films,[20] ZnO nanowires,[21,22] and ZnO nanorods.[23,24] Although several RRS studies have been devoted to analyze the structure property of ZNAs, very few efforts have been made to address RRS in the postannealing effects on the ZNAs grown by low temperature chemical method, particularly to correlate with the change in defects. Beside, compared with the ZnO nanorods grown at higher temperature by the methods of metal-organic chemical-vapor deposition,[25] Catalytic vapor-liquid-solid (CVLS),[26,27] and so on, the low temperature chemically grown ZNAs provide an ideal system to investigate the evolution of surface and bulk defects during the postannealing process.

In this present work, two sets of low temperature chemical grown ZNAs with diameters of 90 and 60 nm annealed under the same condition at temperature from 500 to 700 °C were used for study. The effects of the annealing temperature on the structure and optical properties have been investigated by microphotoluminescence (micro-PL), micro-Raman scattering, and RRS measurements. We particularly utilized the low temperature RRS to monitor, for the first time, to the best of our knowledge, the change in surface defects and deep level defects in the CBD grown ZnO nanorods under thermal treatment from 500 to 700 °C.

II. EXPERIMENTS

The ZNAs used in this investigation were grown on Si substrates by the CBD method, which includes a two-step process, i.e., a substrate treatment prior to the CBD growth. The pretreatment of the substrates, by coating the substrate for different times with a 5 mM solution of zinc acetate dihydrate $[Zn(OOCCH_3)_2 \cdot 2H_2O]$ dissolved in pure ethanol, was used to control the diameter of ZnO nanorods. In the

[a]Author to whom correspondence should be addressed. Electronic mail: lili.yang@itn.liu.se.

CBD growth, the 0.1*M* aqueous solutions of zinc nitrate hexahydrate [$Zn(NO_3)_2 \cdot 6H_2O$, 99.9% purity] and 0.1*M* aqueous solutions of methenamine ($C_6H_{12}N_4$, 99.9% purity) were first prepared and mixed together. The pretreated Si substrates were immersed into the aqueous solution and kept at 93 °C for 2 h. Two samples containing ZNAs on Si (001) substrates with diameters of 90 and 60 nm, respectively, were used in this study. For both ZNAs, a postgrowth thermal treatment was performed at 500, 600, and 700 °C, respectively, for 1 h in air atmosphere and then quenched to room temperature by removing from the oven.

Scanning electron microscopy (SEM) pictures were recorded by using a JEOL JSM-6301F. PL measurements were carried out at room temperature. A charge-coupled device (CCD) detector (Spectrum One) and monochromator HR460 from Jobin Yvon-Spex were used to disperse and detect the ZnO emission. Laser line with a wavelength of 266 nm from a diode laser (Coherent Verdi) pumped resonant frequency doubling unit (MBD 266) was used as excitation source. For resonant Raman measurements, a laser line with 351.1 nm was used. The conventional micro-Raman spectra have been collected in a confocal backscattering configuration under the 100× objective of an Olympus microscope. The 514.5 nm line of a cw Ar–Kr ion laser, Spectra Physics 2060, with a power of 5 mW at the sample position, was used as probe. The cross-polarized scattered radiation was filtered by the first two stages of a triple grating Dilor XY 800 spectrometer, arranged in the subtractive configuration, to remove the strong elastic component, dispersed by the third stage, and recorded by a liquid nitrogen cooled CCD camera (Wright Instruments). Time-resolved PL was performed by using an excitation laser line from a frequency tripled sapphire:Ti laser emitting at 266 nm, a 0.3 m monochromator, and a streak camera at 1.8 K.

III. RESULTS AND DISCUSSIONS

SEM images of the as-grown ZNAs with 90 and 60 nm diameters were shown in Fig. 1. The ZNAs were vertically aligned on the Si (001) substrates. The hexagonally shaped nanorods uniformly covered the entire Si substrate with high density as shown in Figs. 1(a)–1(c). Figure 1(d) illustrated the cross sectional SEM images of ZNAs with 90 nm diameters, from which we can see that the length of the nanorod is about 1.5 μm. After annealing at different temperatures in air, there was no noticeable change in the morphology of the ZNAs used in our experiments.

Raman scattering was used to investigate the annealing effects on the ZNAs crystal quality. Wurtzite ZnO belongs to $C_{6v}^4(P63mc)$ space group, with 2 f.u,/primitive cell. Group theory predicts the existence of the following Raman active phonon modes: $\Gamma = A_1 + E_1 + 2E_2$. Both the A_1 and E_1 modes are polar and split into transverse optical (TO) and longitudinal optical (LO) branches. The A_1 phonon vibration is polarized parallel to the *c*-axis, and the E_1 phonon is polarized perpendicular to the *c*-axis. The two E_2 modes, $E_2(H)$ and $E_2(L)$, are nonpolar modes.

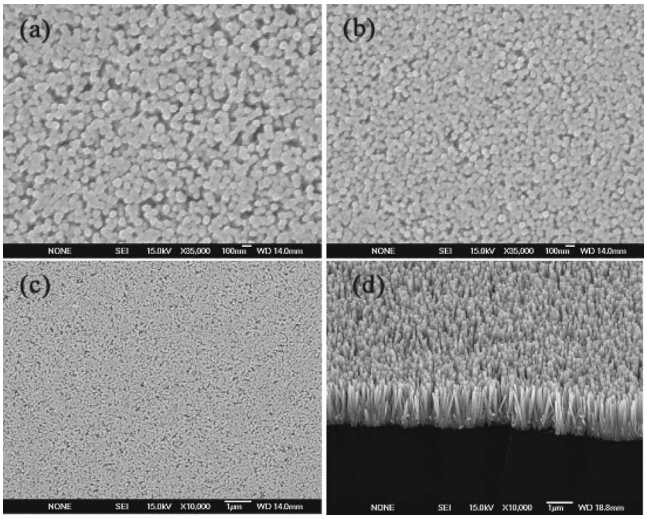

FIG. 1. SEM images of the as-grown samples: (a) 90 nm and (b) 60 nm. (c) Low magnification image of 90 nm diameter ZnO nanorod arrays. (d) Cross sectional image of 90 nm diameter ZnO nanorod arrays.

In our experiments, micro-Raman measurements were carried out at room temperature in a backscattering geometry. That is to say, the spectrum was recorded with the incident light exactly perpendicular to the top surface of the ZNAs, namely, the incident light was parallel to the *c*-axis of the ZnO nanorod arrays. In this configuration, only the E_2 and $A_1(\mathrm{LO})$ modes are allowed, while the $A_1(\mathrm{TO})$ and $E_1(\mathrm{TO})$ modes are forbidden according to the Raman selection rules. Figure 2 illustrates the Raman spectra of ZNAs annealed under different temperatures. For the two sets of samples, the spectra exhibited only $E_2(H)$ and $E_2(L)$ modes at 437 and 99 cm^{-1}, respectively.[28] The $A_1(\mathrm{LO})$ mode expected at 574 cm^{-1} (Ref. 28) has a very small cross section and its contribution from our very thin samples is lost in the noise. The absence of the TO modes in the measurements further confirms that the ZNAs are highly *c*-axis oriented. From Figs. 2(a) and 2(b), one can observe that the annealing temperature had the same influence on the intensity of $E_2(H)$ for the ZNAs with different diameters. The intensity of $E_2(H)$ was strongest for the samples annealed at 500 °C and dropped on both sides toward the as-grown and the 700 °C annealed samples. This indicated that the samples treated at 500 °C had the best crystallization among those measured. However, treatments at higher temperatures are detrimental for the crystallization.

We would like to point out that we also have measured different positions across the samples to do the spatial analysis in order to check the consistency of the spectra across the samples. The results from different positions are similar. This is consistent with the homogeneity of the samples as shown in the SEM imagine [see Fig. 1(c)] and, furthermore, a microscale focusing spot (in our setup, it is about 2.5 μm in diameter) contains many nanorods.

Figure 3 showed the room temperature PL spectrum of the as-grown ZNAs compared to those of samples annealed in air atmosphere at 500, 600 and 700 °C, which consisted of a dominant UV peak at 385 nm in wavelength and a very weak deep level broad emission band in the range of 500–

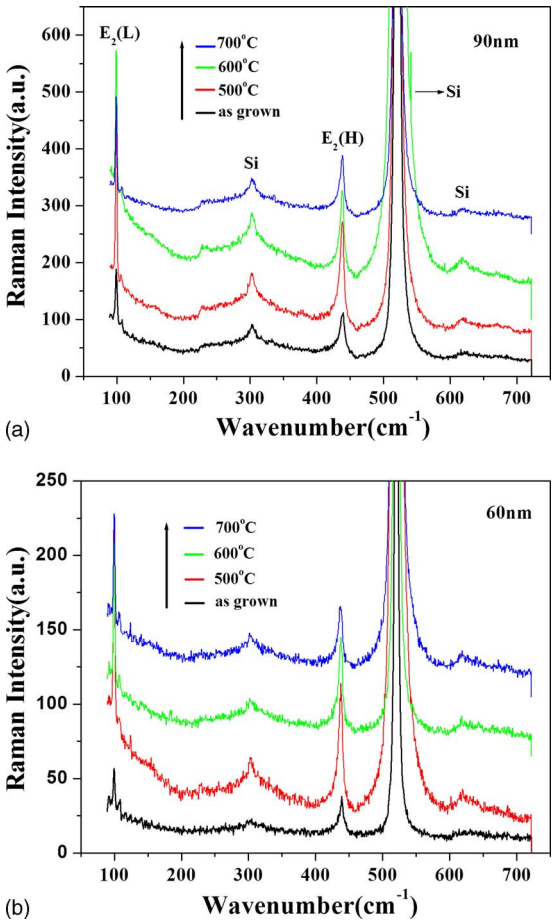

FIG. 2. (Color online) Raman spectra of ZnO nanorod arrays annealed under different temperatures under excitation with wavelength of 514.5 nm at room temperature: (a)90 nm and (b) 60 nm.

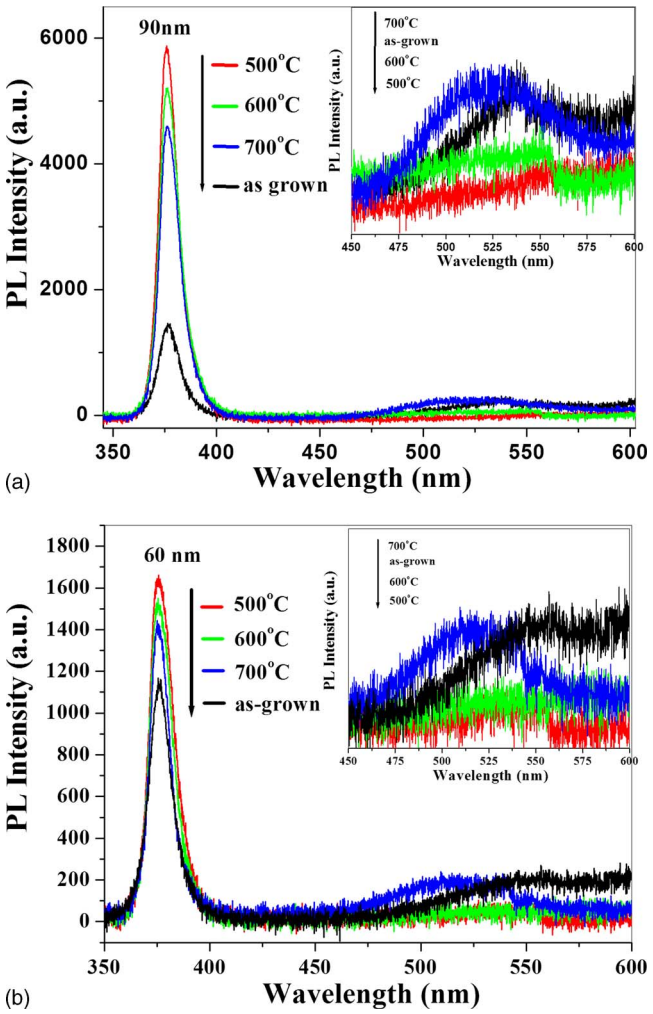

FIG. 3. (Color online) PL spectra of ZnO nanorod arrays annealed under different temperature. The insets show the enlarge part of the PL spectra between 450 and 600 nm: (a)90 nm and (b) 60 nm.

600 nm. The UV emission band is related to a near band-edge transition of ZnO, namely, the recombination of the free excitons (376 nm). The room temperature PL peak position can be different, for example, the transition energy from 375 nm (Ref. 29) to 383 nm,[30] and the exact energy position depends on the contribution between the free exciton and the transition between free electrons to acceptor bound holes.[31–34] The deep level emission band has previously been attributed to several defects in the crystal structure such as O-vacancy (V_O),[35–37] Zn-vacancy (V_{Zn}),[38–40] O-interstitial (O_i),[41] Zn-interstitial (Zn_i),[42] and extrinsic impurities such as substitutional Cu.[43] Recently, this deep level emission band had been identified and at least two different defect origins (V_O and V_{Zn}) with different optical characteristics were claimed to contribute to this deep level emission band.[44–46] From Figs. 3(a) and 3(b), it can be seen that the dependence of the PL intensity versus the annealing temperature showed similar behaviors for the ZNAs with different diameters. Therefore, in the following part we will only discuss the results from 90 nm samples, as shown in Fig. 3(a). After the samples were annealed under 500 °C, a remarkable strong enhancement in UV emission intensity appeared by almost a factor of 4 compared to the as-grown samples and, on the contrary, the deep level emission band almost disappeared. However, after the samples were annealed under 600 and 700 °C, the UV emission intensity decreased and the deep level emission intensity apparently increased step by step again in comparison with the PL spectrum of the sample annealed at 500 °C. One can note the concordance of the PL results and those from the Raman spectra with regard to the effects of annealing on the crystallization.

The relative integrated PL intensity ratio between the UV emission (I_{UV}) and deep level emission (I_{DLE}) can be used to characterize the crystallization of ZNAs.[47] The larger intensity ratio indicates that ZNAs are in better crystallization, i.e., less deep level defects. The relative integrated PL intensity ratio (I_{UV}/I_{DLE}) as a function of various annealing temperatures was summarized in Fig. 4. It can be seen that I_{UV}/I_{DLE} value showed a maximum at the annealing temperature of 500 °C and then decreased again with further increasing annealing temperature. This temperature dependence can be explained from the aspects of the CBD growth mechanism and annealing process, respectively. On the one hand, the surfaces of ZNAs grown with CBD method were prone to absorb various kinds of functional groups. According to the chemical reaction in the solution,[16] these functional groups should be related to the elements such as carbon, nitrogen, and hydrogen. These functional groups had a negative influence on the optical properties of ZNAs. How-

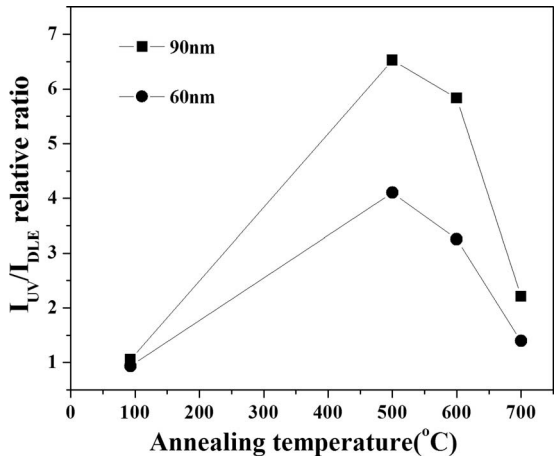

FIG. 4. I_{UV}/I_{DLE} curve via annealing temperature.

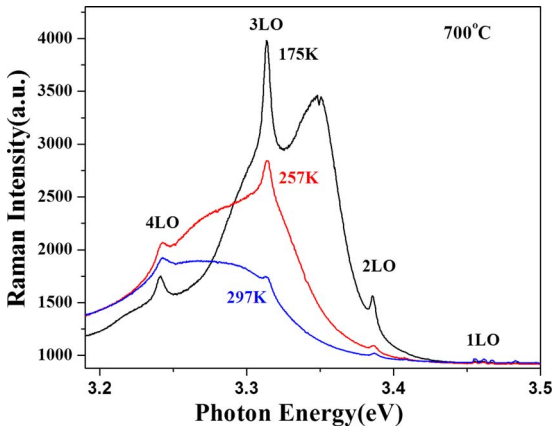

FIG. 5. (Color online) Temperature dependence of emission spectra of ZnO nanorod arrays (90 nm) annealed under 700 °C.

ever after 500 °C annealing for 1 h, all those functional group elements were all released from the surfaces of ZNAs; as a result, the UV emission intensity is strongly enhanced. On the other hand, as mentioned previously, the deep level emission band has been attributed to the presence of large amounts of defects, particularly V_O and V_{Zn} involved complex defects. During the thermal treatment process at high annealing temperatures of 600 and 700 °C, although the absorbed functional group elements were also released from the surfaces of ZNAs, the concentration of defects such as V_O and V_{Zn} also increased due to the thermal diffusion process. Under the same excitation condition, the defect band emission will compete with the UV emission, resulting in that the ZnO nanorods containing more deep level defects give lower UV emission intensity. So the UV emission intensity in those ZNAs after annealing depends on the two competition processes, one is to release the surface attached chemical elements which will enhance the UV emission intensity, and the other is the creation of the deep level defects which will reduce the UV emission intensity. Obviously, deep level defects played a significant role in the emission process of ZNAs annealed in 600 and 700 °C, which can be seen from Fig. 3 that the intensity of deep level emission band increased and the intensity of UV emission band decreased in comparison with the sample annealed at 500 °C. Moreover, the center position of the deep level emission band showed a blueshift, as shown in the inset images in Figs. 3(a) and 3(b), which may be ascribed to the variation in defect species after annealing. The optical property is a reflection of the crystal quality of the samples. The analysis in Fig. 3 showed a good agreement with the results from Raman spectra, which further indicated that the sample after the thermal treatment under 500 °C had the best optical property and crystallization. It was noticed that the structure and optical properties of ZNAs with different diameters in Figs. 2 and 3 exhibited the same tendency. Therefore, we only showed the experimental results from the ZNAs with 90 nm diameter in the following parts.

In order to gain further insight into the defect variation in the ZNAs after thermal treatments, we have investigated the RRS of those samples excited by the 351.1 nm laser line. RRS from solids can be observed if the energy of the incoming or scattered photons matches the real electronic states in the material. This is referred to as incoming and outgoing resonances, respectively.[46] Multiphonon scattering processes were previously reported for single crystalline bulk ZnO,[19] and recently for ZnO films,[20] ZnO nanowires,[21,22] and ZnO nanorods.[23,24] In all these cases the samples were excited by the 325 nm line of a He–Cd laser. The energy of this line is about 440 meV higher than the band gap of ZnO. It means that the laser line is in resonance with an interband electronic transition, i.e., forming incoming resonant condition. In our case, the energy of the 351.1 nm laser line is 160 meV higher than the band gap of ZnO and 200 meV higher than the energy of the free exciton. The energy of this laser line is close to the exciton energy in ZnO, therefore allowing one to investigate the exciton mediated multiphonon RRS under conditions changing from incoming to outgoing resonance.

Figure 5 illustrated the temperature dependence of emission spectra of ZNAs (90 nm) annealed under 700 °C with 351.1 nm excitation. All the spectra consisted of a RRS progression based on a fundamental 1LO band at 3.459 eV and its multiple-LO scatterings. From Fig. 5, one can see that with increasing temperature, the PL band shifted toward lower energies and broadened due to the decrease in the band gap energy. At 175 and 257 K, the photon scattered by third-order phonons matched better the exciton energy and the 3LO peak became the strongest one, while at 297 K, 4LO phonon line became the strongest one. The results clearly illustrated that we deal with pure outgoing RRS and the temperature increase led to the redistribution in the intensity of lines in the RRS in favor of the lines whose energy better matched the exciton energy. Comparing these three spectra in Fig. 5, we can see that the spectrum measured at 175 K shows a strong and a well defined LO phonon scattering. Therefore, we measured the rest of our samples at this temperature.

Since the Raman scattering was performed with backscattering geometry, the main contribution to the RRS signal came from the A_1-LO mode. A_1-LO mode reflected the defect density in the ZnO nanorods. According to the spectra measured under 175 K in Fig. 5, the photon scattered by the 1LO and 2LO phonons were nonresonant with the PL emission, which was correlated only with the concentration

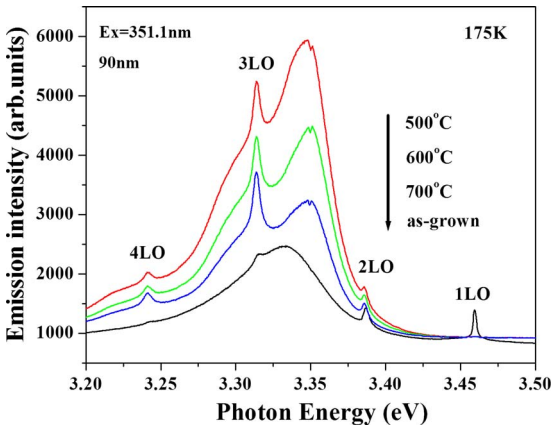

FIG. 6. (Color online) Low temperature emission (175 K) spectra of ZnO nanorod arrays (90 nm) annealed under different temperatures.

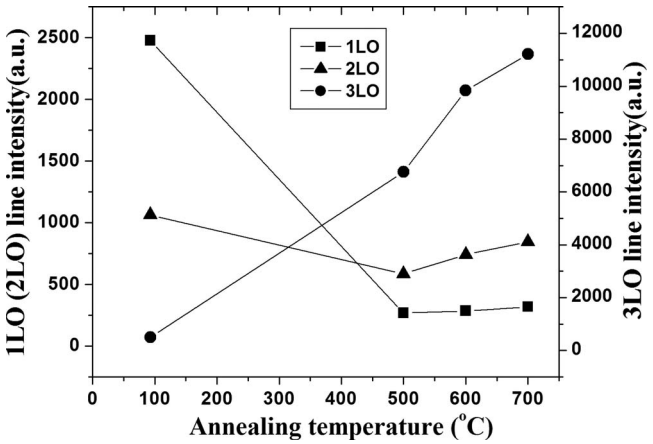

FIG. 7. Dependence of 1LO, 2LO, and 3LO phonon line intensity on the annealing temperature.

change in the defects in the surface and inside of ZnO nanorods, while the photon scattered by the 3LO phonons was in resonance with the PL emission which contained both defect contribution and outgoing resonant effect. So another important reason why we select 351.1 nm excitation and measurement temperature of 175 K is that we would like to distinguish the contribution of surface defect, deep level defects, and the outgoing resonant effect to the optical properties through comparing the intensity variation of single phonon line with annealing temperature.[48]

Figure 6 illustrated the emission spectra of the as-grown and thermal treated ZnO rods under excitation by the 351.1 nm laser line at 175 K. As shown in Fig. 6, it can be clearly seen that the spectrum of the as-grown sample was typical incoming RRS. While the thermal treatment led to a considerable modification of the emission spectra. With the increase in the annealing temperature, a broad and asymmetric PL line emerged on which the RRS lines were superimposed. Simultaneously, a redistribution of the RRS lines intensity occurred. Compared with the spectrum of the as-grown sample, the photon scattered by the third-order LO phonons matched better with the exciton energy and 3LO peak became the strongest one in the spectra of annealed samples, which indicated a transition of RRS from the incoming to the outgoing mode appeared after thermal treatment. This transition can be ascribed to the thermal treatment induced improvement of the optical quality of ZNAs.[49] According to the individual phonon lines in Fig. 6, the intensity of 1LO and 2LO Raman scatterings first strongly decreased in comparison between the as-grown sample and the sample annealed at 500 °C, and then slightly increased as further increasing the annealing temperature. While the intensity of 3LO Raman scattering constantly increased with increasing annealing temperature. In order to see it clearly, the temperature dependences of 1LO, 2LO, and 3LO intensity were illustrated in Fig. 7. The explanation to the variation in these phonon lines via the annealing temperature will be separately discussed in the following parts.

In Fig. 6, in addition to the outgoing resonant effect observed by Ursaki *et al.*,[49] the relative intensity of 3LO phonon lines increased, although the PL emission intensity decreased step by step as the annealing temperature increases from 500 to 700 °C, which was also illustrated in Fig. 7. This tendency was opposite as that observed by Ursaki *et al.*[49] This result indicated that in our case there were different contributions involved in 3LO phonon scattering, observed in Fig. 6. As we know that the outgoing resonance will increase the intensity of Raman scattering, and the increase in the defect concentration will also increase the intensity of Raman scattering. That is to say, the photon could be scattered by not only the third-order LO phonons but also defects. The possibility to enhance the 3LO phone lines will be increased if there are more defects in the samples, which may play an important role in the process of RRS enhancement. According to our case, all the samples originated from one sample. After annealing, we did not observe any significant change in the morphology of ZNAs. The main difference among these samples was the defect concentration in them. According to the results obtained from Figs. 2 and 3, the concentration of defects in ZnO nanorods increased as the annealing temperature increases from 500 to 700 °C, also indicated by the change in 1LO and 2LO phonon intensities in Fig. 6 which will be discussed in more detail below. The intensity variation in 3LO phonon lines corresponds well to the tendency of defect concentration, which means that defects indeed took part in the RRS process and played a significant role. In order to eliminate this defect contribution, the Raman intensity ratio between 3LO and 2LO phonon lines in the RRS spectrum (I_{3LO}/I_{2LO}) was shown in Fig. 8 versus the annealing temperature; for comparison, the intensity of the PL band was also included in the figure. A clear correlation between the dependence of PL band intensity and I_{3LO}/I_{2LO} upon annealing temperature can be observed, which was similar to the result in Ref. 49. Therefore, we believed that both PL intensity and defect scattering should contribute to our results.

It is also believed that the variation in the electron-phonon coupling may influence the relative intensities of the members of the RRS progression in the LO phonon mode.[50,51] However, we have not observed any significant change in the morphology of nanorods induced by thermal treatment. Moreover the diameter of the studied ZnO rods is about 90 nm, which is significantly too large to affect the

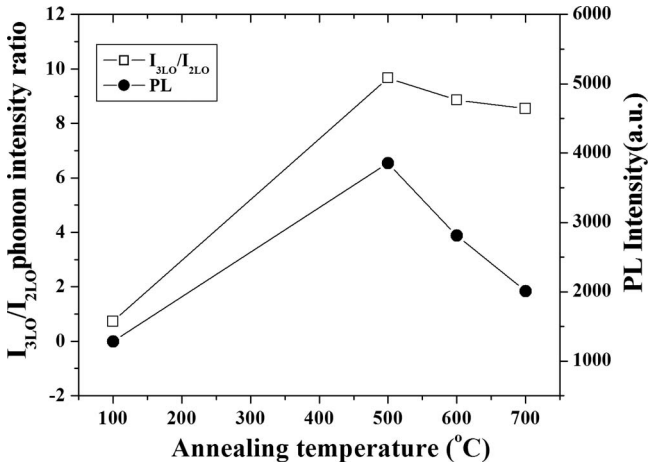

FIG. 8. Dependence of I_{3LO}/I_{2LO} and PL intensity on the annealing temperature.

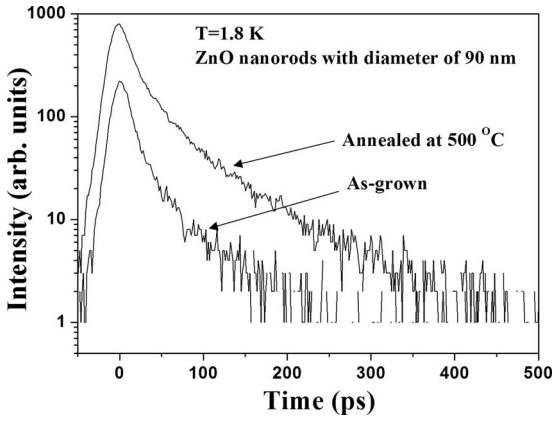

FIG. 9. Decay curves for 90 nm diameter ZnO nanorods from the as-grown sample and after annealing at 500 °C for 1 h. The decays were measured at 1.8 K.

electron-phonon coupling. So the contribution from this mechanism is insignificant in our experiments.

The significant intensity change for 1LO and 2LO peaks in RRS condition in Fig. 6 between the as-grown sample and the sample annealed at 500 °C was another magnificent observation. The 1LO and 2LO Raman intensity (A_1-LO mode) was significantly higher in the as-grown sample, while in nonresonant Raman condition, as shown in Fig. 2, the $E_2(H)$ mode shows an opposite behavior. This was due to the different origin of two Raman modes, i.e., A_1-LO mode reflected the defect density in the ZnO nanorods, while the $E_2(H)$ mode was only related to the optical quality of materials. The strong Raman intensity of 1LO and 2LO (A_1-LO mode) in the as-grown sample indicated that the ZnO nanorods had more defects, resulting also in that the UV emission intensity was significantly weak due to surface defect recombination and relative strong deep level defect emission in comparison with the sample annealed at 500 °C, as also shown in Fig. 3. Further comparison with the samples annealed at 600 and 700 °C, the large Raman intensity of 1LO and 2LO (A_1-LO mode) in the as-grown sample in Fig. 6 and no significant change in the deep level PL emission intensity in Fig. 3 indicated that the surface defects played a significant role in the as-grown sample, as also discussed earlier. The existing surface defects can be further confirmed by time-resolved PL measurement, as shown in Fig. 9.

Figure 9 showed the decay curves from the as-grown sample and the sample annealed at 500 °C. First, the decay measured for annealed sample showed a nonexponential decay. By closely examining the decay curves, the decay can be fitted by two exponential decays, i.e., a fast and a slow decay component. It is clearly shown that the contribution of the fast decay component in the decay curve was strongly suppressed after annealing. There was no observable change in either the crystalline structure of the ZnO nanorods, as deduced from x-ray diffraction curves, or the ZnO nanorod diameter, as concluded from SEM measurements. As demonstrated earlier for Si epilayers,[52] the surface recombination can strongly influence the decay time. The near band gap recombination will exhibit a nonexponential or a single exponential decay, depending on whether the surface recombination is the major recombination channel or not. Therefore, the time-resolved measurements clearly indicated the existing surface defects in the as-grown ZnO nanorods, and the surface defect induced recombination can be strongly suppressed by thermal annealing. By correlating the Raman measurements, PL measurements, and time-resolved PL measurements, we can conclude that the surface defects have a significant contribution to the observed strong Raman intensity of 1LO and 2LO (A_1-LO mode) in the CBD as-grown samples.

IV. CONCLUSIONS

In this paper, the effects of annealing temperature on the structure and optical properties of ZNAs were investigated in detail. The results clearly indicated that the postgrowth thermal treatment at 500 °C in air resulted in the CBD grown ZNAs with good crystal structure and good optical properties. We also utilized the Raman spectroscopy and low temperature PL measurements to identify, for the first time, to the best of our knowledge, the surface defect contribution and outgoing resonant effect in RRS. Furthermore, the Raman measurements can be used to monitor the change in surface defects and deep level defects in the CBD grown ZnO nanorods under thermal treatment from 500 to 700 °C. The results of our investigation provided an effective way to improve the optical properties of low temperature chemical grown ZNAs, which will play an important role to prompt its practical application in the future.

ACKNOWLEDGMENTS

The authors would like to acknowledge financial support for this work from the Foundation for Strategic Research (SSF), the Swedish Research Council (VR), and financial support through NANDOS project from European Commission. L. L. Yang would also like to acknowledge financial support from National Natural Science Foundation of China (NNSFC) (Grant Nos. 60878039 and 60778040).

[1] S. Iijima, Nature (London) **354**, 56 (1991).
[2] M. H. Huang, S. Mao, H. Feick, H. G. Yan, Y. Y. Wu, H. Kind, E. Weber, R. Russo, and P. D. Yang, Science **292**, 1897 (2001).

[3]J. Y. Li, X. L. Chen, H. Li, M. He, and Z. Y. Qiao, J. Cryst. Growth **233**, 5 (2001).
[4]Z. W. Pan, Z. R. Dai, and Z. L. Wang, Science **291**, 1947 (2001).
[5]J. J. Wu, S. C. Liu, C. T. Wu, K. H. Chen, and L. C. Chen, Appl. Phys. Lett. **81**, 1312 (2002).
[6]B. D. Yao, Y. F. Chan, and N. Wang, Appl. Phys. Lett. **81**, 757 (2002).
[7]J. S. Lee, K. Park, M. I. Kang, I. W. Park, S. W. Kim, W. K. Chom, H. S. Han, and S. Kim, J. Cryst. Growth **254**, 423 (2003).
[8]Q. X. Zhao, P. Klason, and M. Willander, Appl. Phys. A: Mater. Sci. Process. **88**, 27 (2007).
[9]M. H. Huang, Y. Wu, H. Feick, N. Tran, E. Weber, and P. Yang, Adv. Mater. (Weinheim, Ger.) **13**, 113 (2001).
[10]Y. Sun, G. M. Fuge, and M. N. R. Ashfold, Chem. Phys. Lett. **396**, 21 (2004).
[11]J. Wu and S. C. Liu, Adv. Mater. (Weinheim, Ger.) **14**, 215 (2002).
[12]W. I. Park, D. H. Kim, S. W. Jung, and G. C. Yi, Appl. Phys. Lett. **80**, 4232 (2002).
[13]H. D. Yu, Z. P. Zhang, M. Y. Han, X. T. Hao, and F. R. Zhu, J. Am. Chem. Soc. **127**, 2378 (2005).
[14]L. Vayssieres, K. Keis, S. E. Lindquist, and A. Hagfeldt, J. Phys. Chem. B **105**, 3350 (2001).
[15]L. Vayssieres, Adv. Mater. (Weinheim, Ger.) **15**, 464 (2003).
[16]L. L. Yang, Q. X. Zhao, and M. Willander, J. Alloys Compd. **469**, 623 (2009).
[17]H. S. Kang, J. S. Kang, J. W. Kim, and S. Y. Lee, J. Appl. Phys. **95**, 1246 (2004).
[18]W. M. Kwok, A. B. Djurišić, Y. H. Leung, D. Li, K. H. Tam, D. L. Phillips, and W. K. Chan, Appl. Phys. Lett. **89**, 183112 (2006).
[19]J. F. Scott, Phys. Rev. B **2**, 1209 (1970).
[20]X. T. Zhang, Y. C. Liu, Z. Z. Zhi, J. Y. Zhang, Y. M. Lu, D. Z. Shen, W. Xu, G. Z. Zhong, X. W. Fan, and X. G. Kong, J. Phys. D **34**, 3430 (2001).
[21]H. T. Ng, B. Chen, J. Li, J. Han, M. Meyyappan, J. Wu, S. X. Li, and E. E. Haller, Appl. Phys. Lett. **82**, 2023 (2003).
[22]H. M. Cheng, H. C. Hsu, Y. K. Tseng, L. J. Lin, and W. F. Hsieh, J. Phys. Chem. B **109**, 8749 (2005).
[23]S. K. Mohanta, D. C. Kim, H. K. Cho, S. J. Chua, and S. Tripathy, J. Cryst. Growth **310**, 3208 (2008).
[24]H. Q. Le, S. Tripathy, and S. J. Chua, Appl. Phys. Lett. **92**, 141910 (2008).
[25]Y. J. Zeng, Z. Z. Ye, W. Z. Xu, L. P. Zhu, and B. H. Zhao, Appl. Surf. Sci. **250**, 280 (2005).
[26]P. Klason, K. Magnusson, O. Nur, Q. X. Zhao, Q. U. Wahab, and M. Willander, Phys. Scr. **T126**, 53 (2006).
[27]L. L. Yang, J. H. Yang, D. D. Wang, Y. J. Zhang, Y. X. Wang, H. L. Liu, H. G. Fan, and J. H. Lang, Physica E (Amsterdam) **40**, 920 (2008).
[28]R. Cuscó, E. Alarcón-Lladó, J. Ibáñez, L. Artús, J. Jiménez, B. Wang, and M. J. Callahan, Phys. Rev. B **75**, 165202 (2007).
[29]Y. Chen, N. T. Tuan, Y. Segawa, H. Ko, S. Hong, and T. Yao, Appl. Phys. Lett. **78**, 1469 (2001).
[30]W. I. Park, S. J. An, G. C. Yi, and H. M. Jang, J. Mater. Res. **16**, 1358 (2001).
[31]B. P. Zhang, N. T. Binh, K. Wakatsuki, Y. Segawa, Y. Kashiwaba, and K. Haga, Nanotechnology **15**, S382 (2004).
[32]K. Maejima, M. Ueda, S. Fujita, and S. Fujita, Jpn. J. Appl. Phys., Part 1 **42**, 2600 (2003).
[33]Q. X. Zhao, M. Willander, R. E. Morjan, Q. H. Hu, and E. E. B. Campbell, Appl. Phys. Lett. **83**, 165 (2003).
[34]W. I. Park, Y. H. Jun, S. W. Jung, and G. C. Yi, Appl. Phys. Lett. **82**, 964 (2003).
[35]P. H. Kasai, Phys. Rev. **130**, 989 (1963).
[36]K. Vanheusden, W. L. Warren, C. H. Seager, D. R. Tallant, J. A. Voigt, and B. E. Gnade, J. Appl. Phys. **79**, 7983 (1996).
[37]S. Yamauchi, Y. Goto, and T. Hariu, J. Cryst. Growth **260**, 1 (2004).
[38]M. Liu, A. H. Kitai, and P. Mascher, J. Lumin. **54**, 35 (1992).
[39]E. G. Bylander, J. Appl. Phys. **49**, 1188 (1978).
[40]X. Yang, G. Du, X. Wang, J. Wang, B. Liu, Y. Zhang, D. Liu, D. Liu, H. C. Ong, and S. Yang, J. Cryst. Growth **252**, 275 (2003).
[41]J. Zhong, A. H. Kitai, P. Mascher, and W. Puff, J. Electrochem. Soc. **140**, 3644 (1993).
[42]K. Johnston, M. O. Henry, D. M. Cabe, T. Agne, and T. Wichert, Proceedings of the Second Workshop on SOXESS European Network on ZnO, Caernarfon, Wales, UK, 27–30 October 2004 (unpublished).
[43]R. Dingle, Phys. Rev. Lett. **23**, 579 (1969).
[44]Q. X. Zhao, P. Klason, M. Willander, H. M. Zhong, W. Lu, and J. H. Yang, Appl. Phys. Lett. **87**, 211912 (2005).
[45]T. Moe Børseth, B. G. Svensson, A. Yu. Kuznetsov, P. Klason, Q. X. Zhao, and M. Willander, Appl. Phys. Lett. **89**, 262112 (2006).
[46]P. Klason, T. M. Børseth, Q. X. Zhao, B. G. Svensson, A. Y. Kuznetzov, P. J. Bergman, and M. Willander, Solid State Commun. **145**, 321 (2008).
[47]C. C. Lin, S. Y. Chen, and S. Y. Cheng, J. Cryst. Growth **283**, 141 (2005).
[48]P. Y. Yu and M. Cardona, *Fundamentals of Semiconductors* (Springer-Verlag, Berlin, 1996).
[49]V. V. Ursaki, O. I. Lupan, L. Chow, I. M. Tiginyanu, and V. V. Zalamai, Solid State Commun. **143**, 437 (2007).
[50]H. M. Cheng, K. F. Lin, H. C. Hsu, and W. F. Hsieh, Appl. Phys. Lett. **88**, 261909 (2006).
[51]R. P. Wang, G. Xu, and P. Jin, Phys. Rev. B **69**, 113303 (2004).
[52]K. Thölmann, M. Yamaguchi, A. Yahata, and H. Ohashi, Jpn. J. Appl. Phys., Part 1 **32**, 1 (1993).